EVALUATION OF THE TRANSPORT AND DEPOSITION OF FUGITIVE DUST USING LIDAR

Dennis Fitz and David Pankratz
College of Engineering-Center for Environmental Research and Technology
University of California, Riverside
1084 Columbia Avenue, Riverside CA 92507
dfitz@cert.ucr.edu

Russell Philbrick and Guangkun Li
Department of Electrical Engineering
The Pennsylvania State University
University Park, PA 16802
crp3@psu.edu

Proceedings of the U.S. Environmental Protection Agency's
11th Annual Emission Inventory Conference:
Emission Inventories-Partnering for the Future
Atlanta, Georgia April 16-18, 2002

21 pages
2002

Evaluation of the Transport and Deposition of Fugitive Dust Using Lidar

Dennis Fitz and David Pankratz
College of Engineering-Center for Environmental Research and Technology
University of California, Riverside
1084 Columbia Avenue, Riverside CA 92507
dfitz@cert.ucr.edu

Russell Philbrick and Guangkun (Homer) Li
Department of Electrical Engineering
The Pennsylvania State University
University Park, PA 16802
crp3@psu.edu

ABSTRACT

Ambient measurements suggest that source inventories of PM_{10} from geologic sources are overestimated by 50 percent or more. This discrepancy may be due to inaccurate emission calculations and/or due to the rapid deposition of PM_{10} after entrainment into the atmosphere. Tests were conducted during December 2000 and December 2001 using a two-wavelength scanning backscatter lidar to investigate PM_{10} deposition rates from artificially generated fugitive dust. Dust was generated by vehicles on unpaved roads and with a blower dispersing known amounts of finely ground calcium carbonate (paint pigment) or native soil. The size and concentration of the resulting dust plumes were monitored for up to a half-hour and a distance of several kilometers. The changes in these dust plumes' characteristics with time, including particle size and density, were estimated from the relationship between backscatter and extinction for the two wavelengths used. The lidar was calibrated using dust of known size distribution and concentration generated in a contained volume during a set of tests conducted in December 2001. An approximation of the backscatter and extinction signals has been obtained using model calculations that are based upon Mie theory for spherical particles. These models show that the backscatter signal does not depend strongly on the particle density but does depend strongly upon size and wavelength of the scattering radiation. However, the extinction depends strongly on the concentration and size of the scattering particles but not on the wavelength. Therefore, simultaneous measurements of the backscatter and extinction at two different wavelengths should permit analysis to reveal the approximate settling rates for the various types (i.e., sources) of fugitive dust.

INTRODUCTION

Geologic material is a major component of the airborne particulate matter in the western United States. Airborne particulate matter is an air quality concern because:

- Recent studies have associated increases in airborne particulate matter with increased morbidity and mortality, particularly in elderly and respiratory impaired individuals[1,2,3].

- Reduced visibility due to airborne particulate matter has both degraded the aesthetic beauty of natural views and affects activities such as the scheduled operation of air traffic.
- The changes in optical transmission of the atmosphere due to suspended airborne particulate matter alters the radiative energy balance of the Earth's environment.

Source inventories for PM_{10} and $PM_{2.5}$ show that geologic dust should contribute approximately 50% of the $PM_{2.5}$ in the western United States. Ambient measurements show that material of geologic origin typically contribute approximately 10% to the mass concentration[4]. There are several potential reasons for this discrepancy, the primary ones being inaccurate algorithms and data to calculate emission inventories and uncertainties of the lifetime of PM in the atmosphere.

Our primary objective was to characterize the fate (deposition and transport) of PM emissions originating from mechanical disturbance of the soil. The results from the measurements will be used to validate the accuracy of the algorithms used to determine emission inventories from such sources. The study focused on PM from unpaved roads and agricultural tilling. The tests also included artificially generated dust clouds of material of known size distribution to provide a validation of the analysis of the optical scattering properties and the algorithms for deposition of airborne particulate matter. The results will allow for more accurate assessment of such sources to the regional PM concentrations. These assessments will then aid the formulation of cost-effective PM control strategies.

The overall approach was to

- Evaluate several types of dust generation processes that are expected to be potentially significant sources of geologic material contributing to the PM in the San Joaquin Valley of California.
- Evaluate methods for determining the amount of particulate matter entrained and their fate.

The work was done in a test area where the generation conditions were controlled and where backscatter lidar could be safely used in the scanning mode to characterize the distribution of particulate matter. Tests were conducted by generating PM emissions to simulate emissions from vehicular travel on dirt roads and soil tilling operations. A series of individual test runs was conducted with data collected from real-time measurement methods. During several of these test runs, in addition to the real-time measurements, time-integrated samples were collected during several test periods.

RESEARCH ACTIVITY

Experimental

The study was conducted at the University of California, Riverside, Agricultural Field Station in Moreno Valley, CA. The 720 acre facility is relatively level, except for some raised (~10 feet) dirt roads that run between some of the fields. There were no significant sources of PM around the facility. The project team coordinated with the UCR field site staff regarding any planned field plowing to avoid that activity during periods that tests were performed. The prevailing daytime winds were expected to be from the west during December.

Figure 1 shows the layout for the equipment at the site. A background meteorological station measuring wind speed (WS), wind direction (WD), temperature (T) and dew point (DP) was also located at this site. The meteorological tower provided wind speed and direction at 2, 5, and 10 meters, temperature measurements at 2 and 10 meters, and net radiation measurements at 1.5 meters. The signals from the meteorological sensors were scanned once per second by a Campbell CR10X data logger and processed into ten-second averages.

The SESI scanning micro-pulse lidar (MPL) was located 153 meters upwind of the main dust generator during the pilot study in December 2000. It provided the backscatter signal profiles at two wavelengths and has several features that make it the ideal instrument for mapping the dust clouds to be generated in this program. The instrument has a scanning platform, which can be used to provide a mapping of the airborne particulate matter. The instrument is eye-safe but maintains high sensitivity by using high average power, which is obtained by using a high operating pulse repetition frequency (prf), and the beam is expanded to produce lower energy flux per unit area.

The MPL measures the backscatter signal profiles at 1047 nm in the near infrared (NIR) and 523 nm in the mid-visible spectrum. These wavelengths are most sensitive to scattering from particle sizes in the size range near 1 micron, and they are separated sufficiently to provide some sensitivity to changes in fine particle size distributions.

A high-resolution digital video camera (Sony Digital DCR-VX700) was mechanically coupled to the lidar to document the distribution of the dust generated and to verify the lidar position. Images were taken at each scanning position by the camera mounted on the top of the lidar to follow the path of the laser beam and provide a clear picture of the area being scanned. The scanning lidar with the camera was located upwind of the generation point. The scan covered the region about 10-20° on either side of the centerline from the location of the lidar to the generation point. An inclinometer was mounted on the lidar to measure the elevation angle.

A second video camera was used in the program. It was placed at the location shown in Figure 1. Running simultaneously, these two cameras provided a more complete visual representation of the spatial evolution of the dust clouds.

Most of the dust generation releases were performed using a stationary generator as shown in Figure 2. This device used a 5 horsepower centrifugal blower. Limited testing was carried out using calcium carbonate (~10 μm size) and a fogger (propylene glycol) of the type used to provide special effects for the film industry. For the remaining tests, dust was generated by driving a vehicle (Chevrolet Suburban) along the paths shown in Figure 1. Figure 3 shows the dust generated by this vehicle.

Results and Discussion

The dust generation and measurement instruments were made from 11 to 18 December 2000. Dust was generated and monitored for a total of 22 test periods. Ten-second average meteorological measurements, tracer gas releases and sampling, digital and video camera measurements, and lidar measurements were made during these test periods. Dust was generated and monitored for a total of 22 test periods. These included 11 tests with sieved indigenous soil, 4 tests with the white paint pigment powder, 5 tests with vehicle-generated dust, and 2 tests with the fog generator. Table 1 presents a list of test activities and the time periods that those activities were performed.

Figure 4 shows a typical experiment showing photos of the generation of a dust cloud from the digital video camera mounted on top of the lidar. The dust generation equipment was located about halfway between the lidar and the measurement tower. The lidar was used to automatically make horizontal scans of the test volume, and the elevation angle could be adjusted manually. Using the scanning lidar, the plumes were generally tracked out to 1 km along the path and on radials, which were swept up to $\pm 30^{o}$ horizontally. The plumes probably could have been tracked much longer, at least along some radials, up to the lidar's maximum range of 20-30 km. Because it was more desirable to obtain data over shorter distances for the pilot study, tracking of plumes was stopped at about 1.5 km.

Figure 5 shows the results of using scene extraction techniques while following the dust cloud. The image obtained with a digital camera was analyzed by removing the background scene by subtracting, pixel by pixel, a background image obtained just before generating the dust plume. After scene extraction is applied, only the signal due to the dust plume is left. The spatial dimensions indicating growth or drift of the cloud can be extracted. It is also possible to determine the optical depth of the cloud relative to the background scene at times and locations where the path is not optically thick.

Figure 6 shows vertical profiles obtained for the visible and near infrared (NIR) channels when the instrument was pointed on an elevation angle of 70^{o}. The data have been range-corrected for $1/R^2$ (where "R" is the distance from the lidar to the measured plume) dependence, but no other corrections have been applied. Therefore, the telescope form factor is quite noticeable. The top of the planetary boundary layer (PBL) is clearly evident in both the visible and NIR channels. The visible signal is large compared with

the NIR signal, and we would expect that most of the contribution to the scattering is by small particles. The shape of the vertical scattering profile is that expected for a well-mixed atmosphere that is relatively clean. The increase in the signal versus altitude is due to two factors, the telescope form factor and the fact that the particles grow larger as the temperature decreases versus altitude. The increase in relative humidity as a function of altitude causes growth in the size of the particles, and since the optical scattering increases approximately with R^6 (where "R" is the radius of the particle) for small particles, we expect to observe more optical scattering near the top of the boundary layer.

Figure 7 shows the returns measured from a target board at a distance of 660 m from the lidar. The measurement was made on four occasions and the results show that no major changes in performance occurred during the period. The differences can be attributed to changes in the path transmission.

Figures 8 and 9 show examples of the measurements from the two wavelengths. The results shown in Figure 8 display the backscatter and the extinction. The backscatter is larger for the NIR channel and the extinction is larger for the visible channel. These differences provide a foundation for using the lidar data to describe and characterize the changes in the airborne particulate matter. Figure 9 shows the large range of changes in backscatter and extinction as the concentration of particles changes during the generation of a very dense cloud using the spinning tire of a vehicle along a 50 m long north-south line. The results are plotted relative to the atmospheric profile immediately before the test to show the dust characteristics more clearly. During the 45-second generation period, the extinction increased and then rapidly decreased again as the larger particles settled quickly, and the fine particle component is observed later. Notice that the extinction reaches a maximum value near the end of the generation period and then decreases rather rapidly. The rapid recovery of the extinction is due to the more rapid settling out of the larger particles; however, the number density is largely composed of smaller particles that stay airborne longer and contribute to the backscatter signal.

The laser signal strength is attenuated after passing the dust cloud. As shown in Figure 8 comparing with the backscatter signal before the dust was generated, the signal strength starts increasing at the front edge of dust plume and forms a peak in the center of cloud. The backscatter coefficient can be estimated from the peak's magnitude. After the laser beam passes through the cloud, there is a sudden drop of backscatter signal due to the attenuation of the laser beam. The extinction coefficient can be estimated by the attenuation amount, which is the signal drop after the laser signal passing through the dust plume. If we assume the dust particles inside the cloud are uniform and spherical, a certain relationship should exist between the values of backscatter and extinction coefficients that correspond to a dust plume with given set of particle sizes. This will allow us to simulate the laser backscatter profile passing through the cloud and specify the dust particle size and density from the analysis of the simulation.

A simple model calculation based upon the scattering theory for spherical particles by Gustov Mie has been used to simulate first order effects observed. Mie theory

calculations provide the scattering angle dependence for spherical particles with various indices of refraction[5]. While the dust scattering studied in these experiments cannot be described as associated with spherical particles, it still provides a useful comparison of the scattering properties. In particular, the Mie theory results should provide accurate results for the smaller particles, where shape is less important, and the relationship between the forward and backward scatter intensities (extinction and backscatter) should provide useful insight for this investigation. The theory also provides information on the variations in the absorption of the particles due to their complex index of refraction. The Mie scattering theory used for this investigation is a straightforward application of the scattering intensity in the two polarization planes that comes from directly from electromagnetic theory, and all of the applications here use only the 0^o and 180^o scattering intensity.

Figure 10 shows model calculations of visible and NIR backscatter and extinction for 10μm diameter particles for a variety of concentrations. The calculation simulates a 200-meter-thick uniform dust cloud and calculates values at 30-meter intervals (same as the bin size of the lidar result). The figure shows the differences in backscatter and extinction signals as the density concentration of 10 μm particles changes. It is important to notice that the extinction only depends on the concentration of particles and not the wavelength or absorption. However, the backscatter does depend strongly on the wavelength, but it does not depend on the particle density as long as the dust does not become optically thick.

The calculations shown in Figure 11 demonstrate that the backscatter intensity and the extinction depend on the particle size. The relatively larger backscatter for the NIR wavelength is expected based upon the fact that the longer wavelength allows the particles to remain longer in the Rayleigh scattering range, where the cross-section dependence ($r^6 \sim 2^6 = 64$) results in increased scattering. Increasing the particle size increases the backscatter up to the point where the scattering loss results in an optical thickness that reduces the backscatter signal.

Figure 12 shows one example from the December 2001 test for the case of a 10 μm calcium carbonate cloud containing 600 grams of material. Notice that the magnitude of the backscatter and extinction are similar to the values in the simulation for 10 μm particles shown in Figure 11(a). After release, the backscatter signal does not change very much during the next two minutes (4 profiles) and the extinction is observed to slowly recover. The 10 μm material is sufficiently small that the settling time is slow when compared with the rapid recovery of the extinction from larger dust particles generated by a vehicle in Figure 9.

The experimental backscatter and extinction measurements can now be examined in the context of the simulation calculations. The more difficult task is to use the field measurements to solve the inverse problem and describe the particulate matter properties from the scattering profiles. Our goal is to describe size and distribution of the air borne PM and to show the variation in the settling rate of the particulate matter from various sources. The analysis aimed at developing the inversion algorithm for fully describing the

changes in particle size within the generated dust clouds is under way as part of the Ph.D. dissertation of one of us (Guangkun Li) and it is expected to be completed during the coming months.

CONCLUSIONS

Optical scattering measurements using lidar have been examined for each of the several tests using native soil and sized calcium carbonate to generate clouds, and some examples of these results are presented here. The model calculations show that extinction is more dependent on concentration and backscatter is more dependent on particle size. Based on the analysis of results obtained thus far, it is expected that settling rates for generated fugitive dust of various types will be estimated from the lidar data obtained. The preliminary indication is that the rapid settling rate of the larger particles (even when the significant backscatter from the longer airborne small particles is present) results in the lower quantity of fugitive dust as a fraction of emission inventory.

REFERENCES

1 Magari, S.R.; Hauser, R.; Schwartz, J.; Williams, P.L.; Smith, T.J.; and Christiani, D.C. Association of heart rate variability with occupational and environmental exposure to particulate air pollution. *Circulation* 104, 986-991, 2001.

3 Mauderly, J.; Neas, L.; and Schlesinger R. PM monitoring needs related to health effects. *Proceedings of the PM Measurements Workshop*, EPA Report No. 2, Chapel Hill, NC, pp 9-14, July 1998.

2 Peters, A.; Dockery, D.W.; Muller, J.E.; and Mittleman, M.A. Increased particulate air pollution and the triggering of myocardial infarction. *Circulation* 103, 2810-2815, 2001.

4 Watson, J.G., and Chow, J.C. Reconciling Urban Fugitive Dust Emissions Inventory and Ambient Source Contribution Estimates: Summary of Current Knowledge and Needed Research. Document No. 61110.4D2, Desert Research Institute, Reno NV, September 3, 1999.

5 Li, G.; Kizhakkemadam, S.N.; and Philbrick, C.R. Optical scattering by airborne dust particles. Proceeding of the Air Force Optical Transmission Meeting, Hanscom AFB, MA June 2001.

ACKNOWLEDGEMENTS

We wish to thank Patrick Gaffney and the California Air Resources Board for funding this research. We appreciate Tony Taliaferro's assistance in setting up the equipment

used in this study. The efforts of Sriram Kizhakkemadam and Gregg O’Marr contributed to the lidar results and were important for the successful data collection.

DISCLAIMER

The statements and conclusions in this report are those of the researchers and universities and not necessarily those of the California Air Resources Board. The mention of commercial products, their source, or their use in connection with material reported herein is not to be construed as actual or implied endorsement of such products.

Figure 1. Lot plot showing measurement equipment layout.

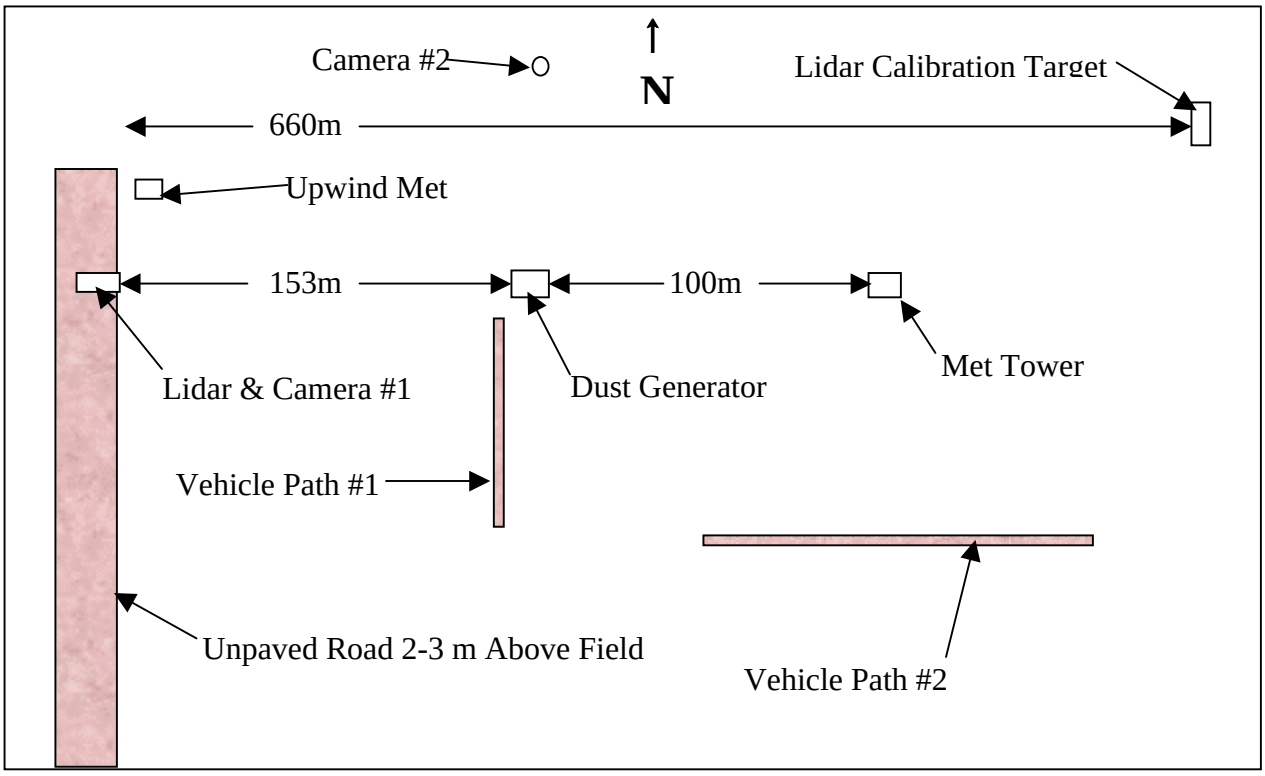

Figure 2. Photograph of centrifugal blower dust generator.

Figure 3. Photograph of vehicular dust.

Figure 4. A set of the digital images selected from Test #2 to illustrate the growth of a dust cloud using the imaging data.

Figure 5. Time sequence of CCD images for Test #18 (dust generated with a vehicle) along with the corresponding background removed images. (a) 14:31:37 (b) 14:32:36 (c)14:32:49 (d) 14:33:14.

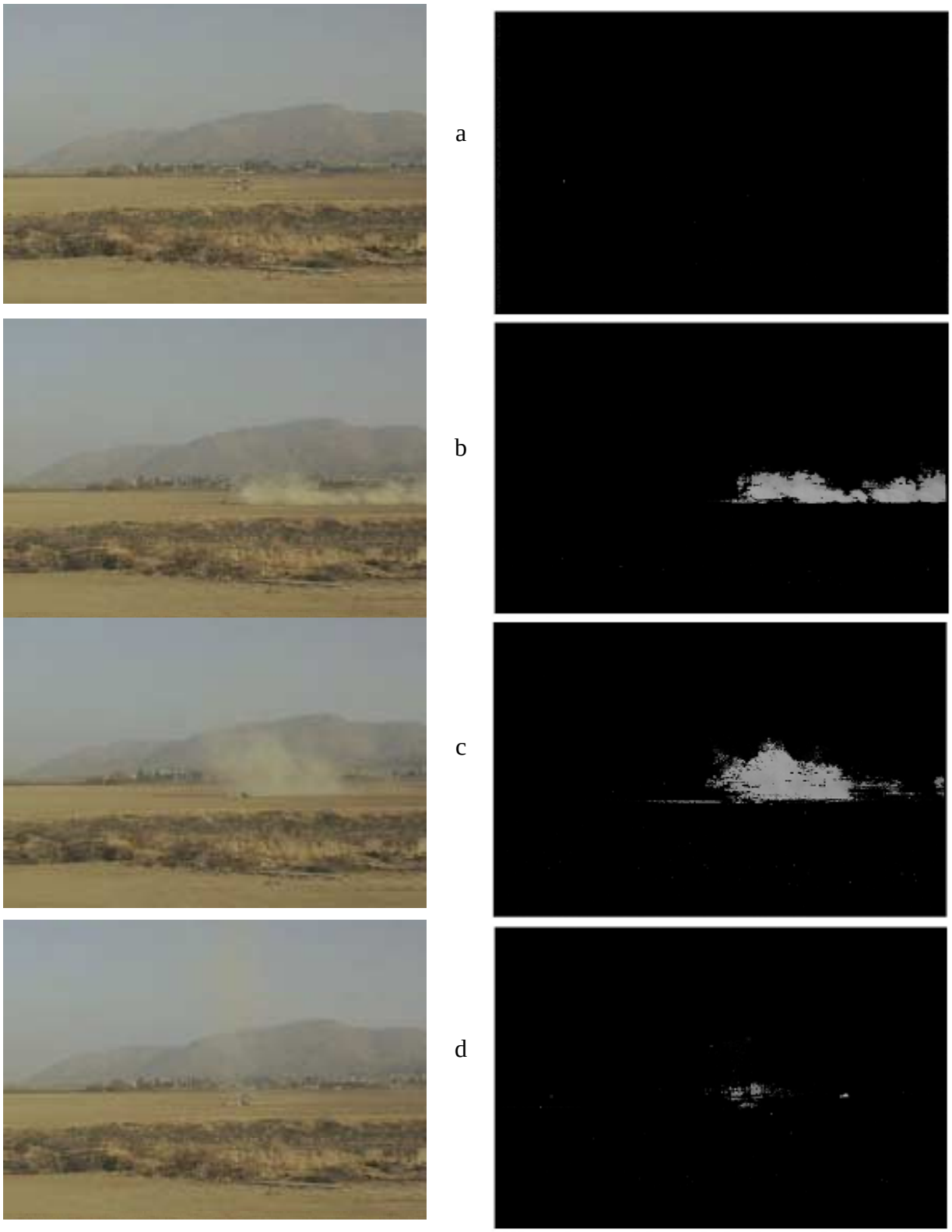

Figure 6. Vertical profile (elevation angle 70^{o}) during period of afternoon convection shows the top of the boundary layer near 1300 m.

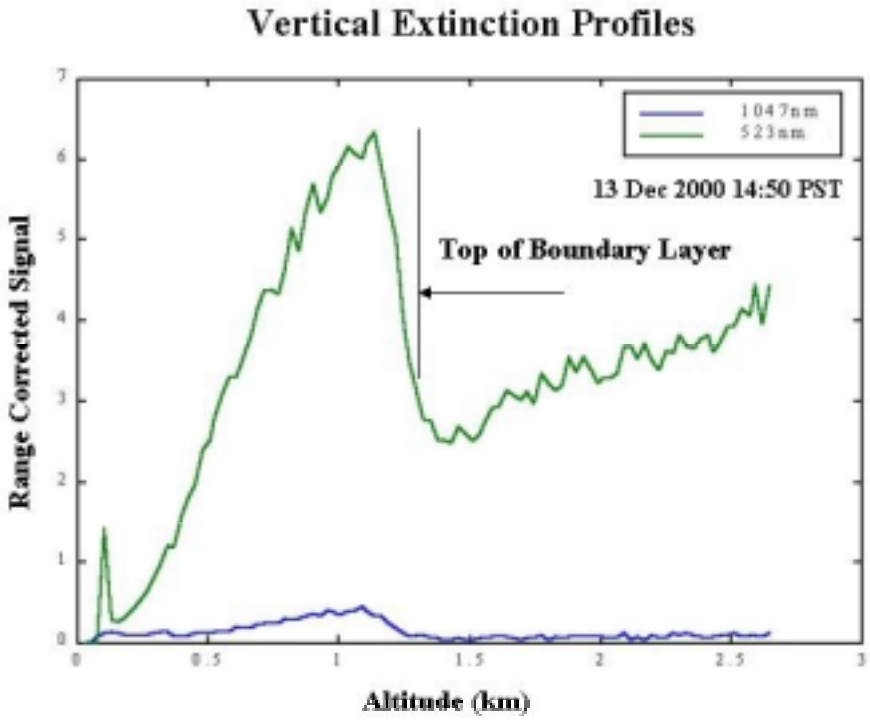

Figure 7. Return from target board at distance of 660 m was used to check the instrument performance and the measure the return as an indication of optical transmission changes.

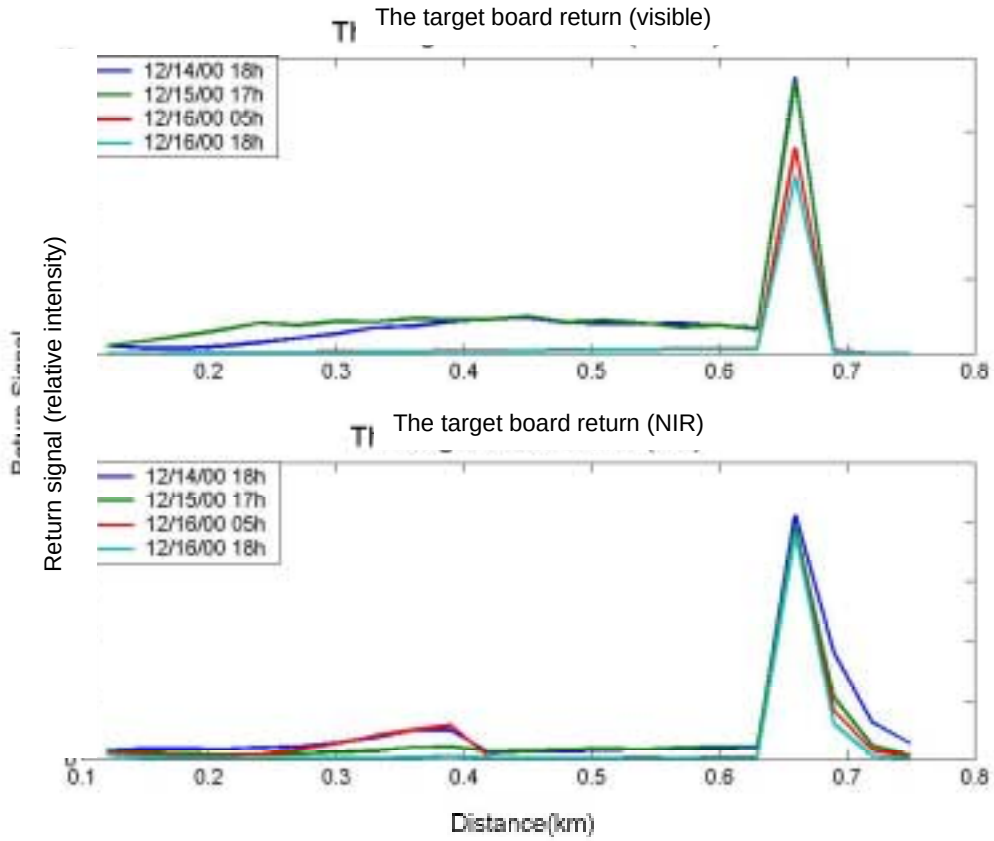

Figure 8. Examples of the raw data profiles from the lidar at the visible and NIR wavelengths during Test #4 show the backscatter and extinction associated with a dust plume at a range of about 500 m.

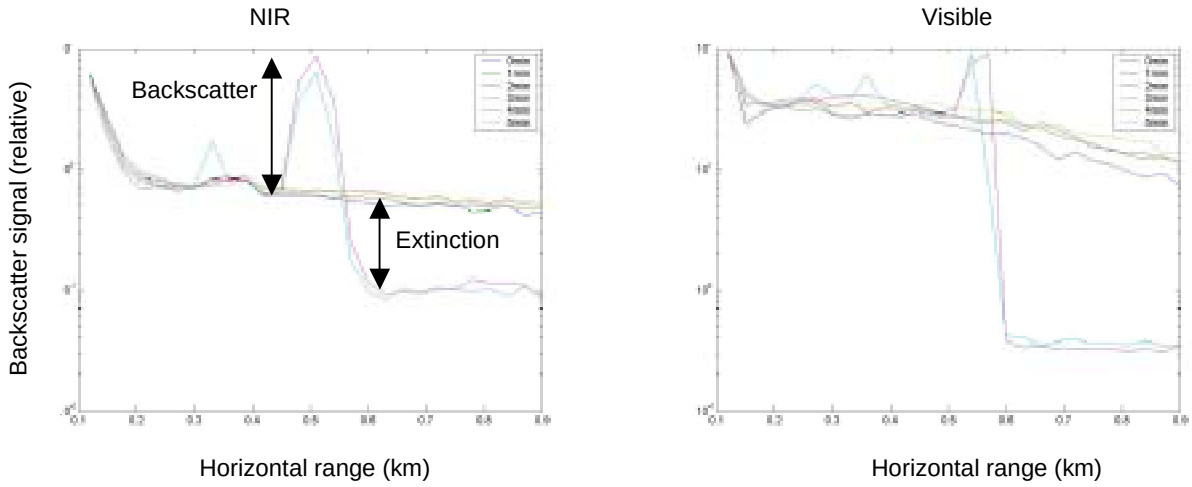

Figure 9. The backscatter and extinction at both visible and NIR wavelengths resulting from vehicle generated dust between 14:32:00 and 14:32:45 during Test #18.

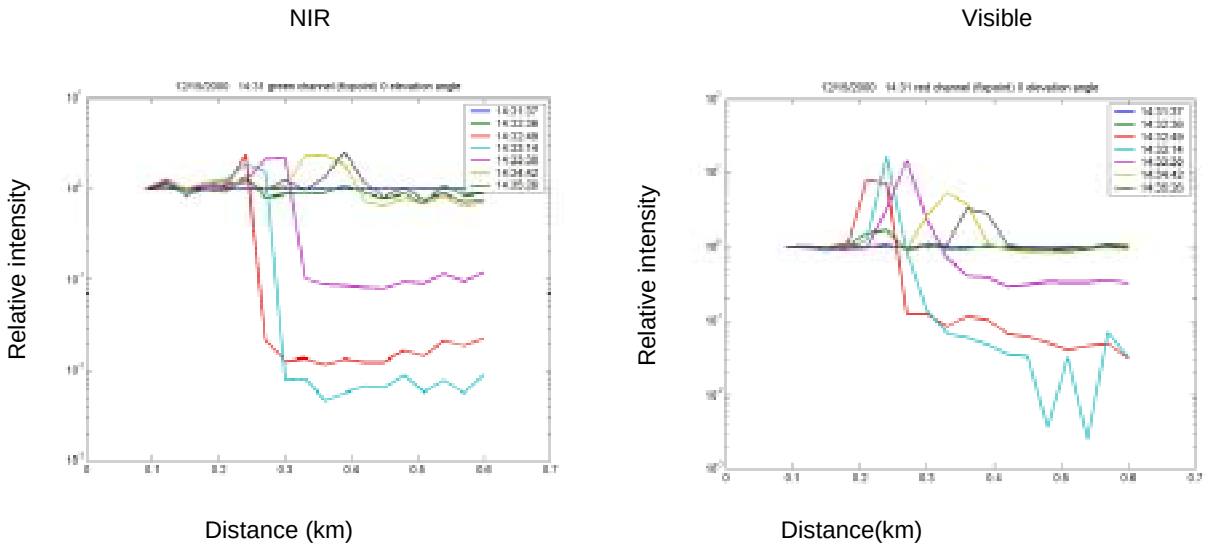

Figure 10. Simulation of the scattering from 10 μm dust for a model calculation shows the expected backscatter and extinction profiles for both wavelengths at several different particle concentrations in the upper panels.

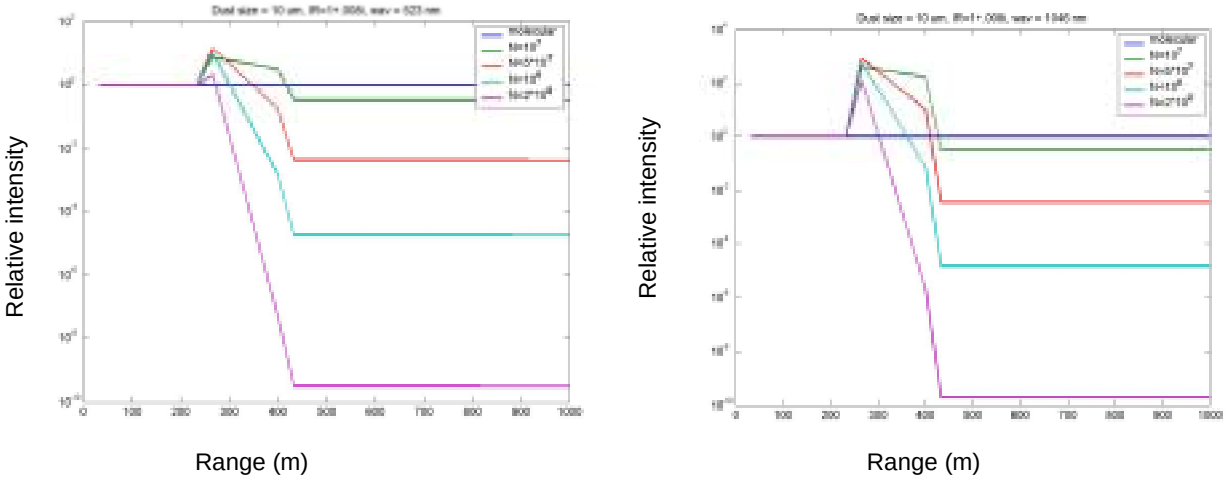

Figure 11. The calculations of the backscatter and extinction profiles for the two wavelengths are shown as the particle size changes. The upper panels show values for particle concentration of 10^7 m^{-3} and the lower panels for concentration of 10^8 m^{-3}.

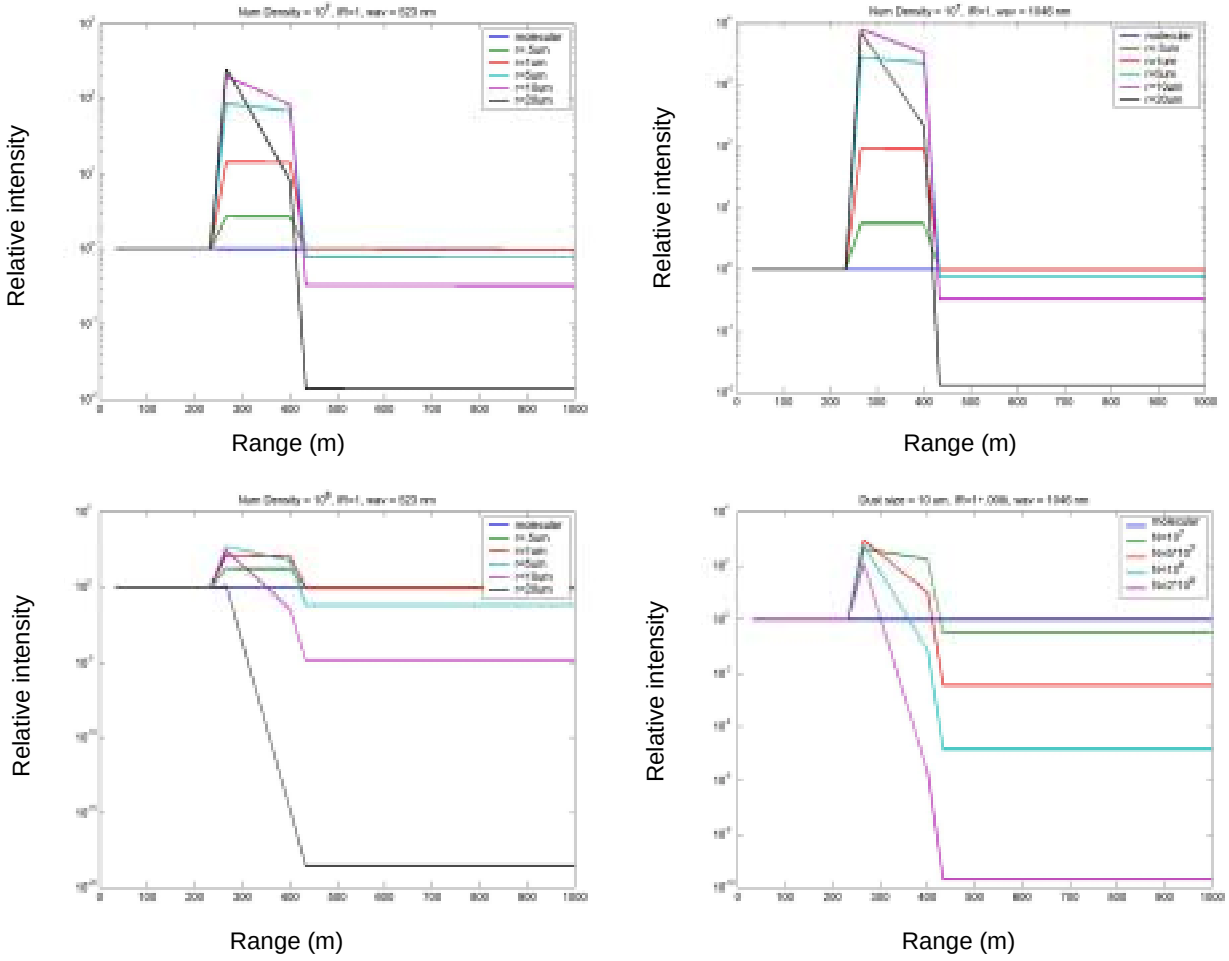

Figure 12. Example of December 2001 test for the case of a 10 μm calcium carbonate cloud containing 600 grams of material.

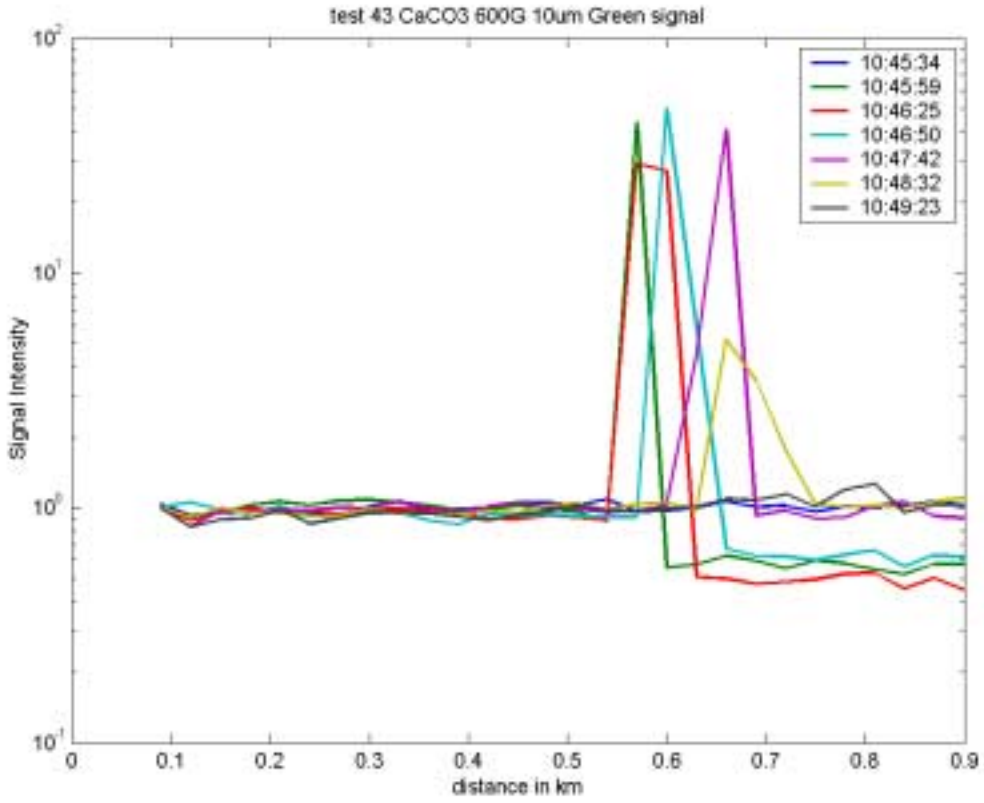

Table 1. Test activities log.

Event	Date	Start Time (hr:mn:sec)	Duration of Release (min:sec)	Release (Kg)	Dust Generation Material
1	12/13/2000	15:08:05	0:05	0.54	Sieved indigenous soil
2	12/13/2000	16:31:00	0:50	5.50	Sieved indigenous soil
3	12/14/2000	10:55:00	1:10	5.00	Sieved indigenous soil
4	12/14/2000	11:40:00	0:50	5.00	Sieved indigenous soil
5	12/14/2000	12:11:00	12:29	22.00	Sieved indigenous soil
6	12/14/2000	14:59:30	1:10	4.42	White paint pigment powder
7	12/14/2000	15:15:30	2:45	5.04	White paint pigment powder
8	12/14/2000	15:46:00	3:15	4.66	White paint pigment powder
9	12/14/2000	16:11:00	1:10	5.00	Sieved indigenous soil
10	12/14/2000	16:31:00	1:30	5.00	Sieved indigenous soil
11	12/14/2000	16:55:00	1:30	5.00	Sieved indigenous soil
12	12/14/2000	17:21:00	1:30	5.00	Sieved indigenous soil
13	12/14/2000	17:45:00	1:30	5.00	Sieved indigenous soil
14	12/15/2000	11:48:00	1:30	1.50	Sieved indigenous soil
15	12/15/2000	12:02:00	1:00	1.45	White paint pigment powder
16	12/15/2000	12:13:00	~20 sec		Suburban; drove around upwind of tower
17	12/15/2000	14:18:00	~20 sec		Suburban; 50 meter line source
18	12/15/2000	14:32:00	~20 sec		Suburban; down/back over 50 meter line (N-S)
19	12/15/2000	15:14:00	~20 sec		Suburban; 150 meter line (E->W)
20	12/15/2000	15:25:00	1:00		one minute "fog" release
21	12/15/2000	15:30:00	1:00		one minute "fog" release
22	12/16/2000	12:15:00	~20 sec		Suburban; N->S line release